ELSEVIER

Journal of Alloys and Compounds 446–447 (2007) 620–624

Journal of ALLOYS AND COMPOUNDS

www.elsevier.com/locate/jallcom

Stacking structures and electrode performances of rare earth–Mg–Ni-based alloys for advanced nickel–metal hydride battery

T. Ozaki [a], M. Kanemoto [b], T. Kakeya [b], Y. Kitano [a], M. Kuzuhara [b], M. Watada [b], S. Tanase [a], T. Sakai [a,*]

[a] *National Institute of Advanced Industrial Science and Technology (AIST), Kansai Center, 1-8-31 Midorigaoka, Ikeda, Osaka 563-8577, Japan*

[b] *GS Yuasa Corporation, Nishinosho, Kisshoin, Minami-ku, Kyoto 601-8520, Japan*

Received 30 September 2006; received in revised form 8 March 2007; accepted 9 March 2007
Available online 19 March 2007

Abstract

Rare earth–Mg–Ni-based alloys with stacking structures consisting of AB_5 unit ($CaCu_5$-type structure) and A_2B_4 unit (Laves structure) have received attention as negative electrode materials for advanced nickel–metal hydride (Ni–MH) battery. These alloy materials are very attractive because of high hydrogen storage capacity, low cobalt content and moderate plateau pressure, but have some difficulty to control the phase abundance and electrode performances. In this paper, relationship among composition, phase abundance, and electrochemical properties was investigated. Structural analysis was done using synchrotron X-ray diffraction patterns. In alloys such as $La_{0.8}Mg_{0.2}Ni_{3.4-x-y}Co_{0.3}(MnAl)_x$ ($0 \le x \le 0.4$), phase abundance was drastically changed with increasing amount of Mn and Al. In the range of $0.1 < x \le 0.2$, hexagonal Pr_5Co_{19}-type (5:19H) or rhombohedral 1:4R phases were dominant. The Rietveld analysis suggested that Mg occupies La sites in A_2B_4 unit, and Al has tendency to occupy Ni sites between A_2B_4 unit and AB_5 unit or between AB_5 units in these types of phases. The developed alloys showed higher discharge capacity by 20% than the conventional one at a 0.2 C discharge rate.

Keywords: Hydrogen storage alloy; Nickel–metal hydride battery; Multi-phase structure; Synchrotron XRD measurement; Rietveld analysis

1. Introduction

Nickel/metal hydride (Ni/MH) battery has advantages such as compact, lightweight, and high power output, and its application field has been extended from mobile devices such as a digital camera to hybrid electric vehicle (HEV). Discharge capacity and energy density of Ni/MH battery have increased year by year. As a negative electrode for Ni/MH battery, AB_5-type alloys consisting of rare earth elements, Ni, Mn, and Al have been used. The discharge capacity of them has reached about 85% of theoretical one of $LaNi_5$ (372 mAh/g), and it is difficult to increase the capacity more using this alloy system.

In recent years, rare earth–Mg–Ni-based alloys attract attention as an electrode material for Ni/MH battery, because of their high hydrogen storage capacity and moderate hydrogen equilibrium pressure. Many high-capacity alloys have been reported in the composition range of $AB_{3.0}$–$AB_{4.0}$ (A: rare earth, Ca, and Mg, B: transition metals and Al). These alloys have long-periodic one-dimensional superstructures, in which AB_5 unit ($CaCu_5$-type structure) and A_2B_4 unit (Laves structure) are rhombohedrally or hexagonally stacked with ratio of n:1 along the c-axis direction. In 1997, Kadir and Sakai et al. have discovered $REMg_2Ni_9$ (RE: rare earths) alloys with $PuNi_3$-type structure: rhombohedral 1:1 stacking of the AB_5 and A_2B_4 units. Partial substitution of RE and Mg with Ca in $(RE_{1-x}Ca_x)(Mg_{1-y}Ca_y)_2Ni_9$ increased hydrogen storage capacity to about 1.9 wt.% and discharge capacity to about 370 mAh/g [1–6]. Pan et al. also investigated various La–Mg–Ni–Co alloys with $PuNi_3$-type structure [7]. Kohno et al. developed $La_{0.7}Mg_{0.3}Ni_{2.8}Co_{0.5}$ alloy with $La_5Mg_2Ni_{23}$-type structure: hybrid of 1:1 and 2:1 stacking. This alloy showed high hydrogen storage capacity of H/M = 1.1 and high dis-

* Corresponding author.
E-mail address: sakai-tetsuo@aist.go.jp (T. Sakai).

0925-8388/$ – see front matter © 2007 Published by Elsevier B.V.
doi:10.1016/j.jallcom.2007.03.059

charge capacity of 410 mAh/g [8]. Yasuoka et al. developed $Mm_{0.83}Mg_{0.17}Ni_{3.1}Al_{0.2}$ (Mm: mischmetal) alloy with Ce_2Ni_7-type structure: hexagonal 2:1 stacking. This alloy electrode showed discharge capacity of about 340 mAh/g and good cycle life in the test using AA-sized sealed cell [9]. Hayakawa et al. investigated crystal structures of $La_{0.7}Mg_{0.3}Ni_{2.5}Co_{0.5}$ and $La_{0.75}Mg_{0.25}Ni_{3.0}Co_{0.5}$ alloys, and identified Ce_5Co_{19}-type and Pr_5Co_{19}-type structures, which are rhombohedral and hexagonal 3:1 stacking, respectively [10]. These previous results suggest that stacking structure and electrode properties of the rare earth–Mg–Ni-based alloys would be dependent on their atomic composition.

We have investigated relationship among alloy composition, crystal structure (phase abundance), and electrode properties for the rare earth–Mg–Ni-based alloys in the composition range of $AB_{3.0}$–$AB_{4.0}$, and found that the alloys with composition ratio of $AB_{3.7}$ showed discharge capacity of 360 mAh/g [11,12].

In the present study, crystal structures of rare earth–Mg–Ni-based electrode alloys with composition ratio of $AB_{3.7}$ were investigated in the charge–discharge state using synchrotron X-ray diffraction (XRD) patterns. The most suitable alloy composition for the electrode is discussed.

2. Experimental

$La_{0.6}RE'_{0.2}Mg_{0.2}Ni_{3.4-x}Co_{0.3}(MnAl)_x$ (RE′: La, Pr, and Y, $0 \le x \le 0.4$) alloys were prepared by induction melting, and were then annealed at 900–1000 °C. Microstructures of the alloy ingots were observed by scanning electron microscope (SEM)-electron probe microanalyzer (EPMA). The alloys were then crushed into average particle size of about 20 μm. The XRD samples were prepared by sealing the alloy powder into Lideman glass capillary with 0.3 μm of inner diameter. Synchrotron XRD measurements were carried out using a large-diameter Debye–Scherrer camera with an imaging plate at Spring8 BL19B2 beam line (wavelength 0.7 Å). The alloy phases were identified using the obtained XRD patterns. By means of Rietveld analysis (software: RIETAN-2000 [13]), lattice parameters of the phases were refined, and their phase abundances were determined. Hydrogen absorption–desorption characteristics were evaluated by measuring pressure–composition–temperature (*P–C–T*) curves using Sievert type apparatus at 80 °C. Paste-type electrodes were prepared by using the alloy powder, Ni powder as a conductive agent, styrene butadiene rubber (SBR) as a binder, and nickel-plated punched sheet (NPPS) as a substrate. The test cell was assembled using the negative electrode and sintered-type nickel electrode, and tested at 0.2 C rate to evaluate electrochemical properties.

3. Results and discussion

In the prepared rare earth–Mg–Ni-based alloys four kinds of stacking-structured phases such as rhombohedral Gd_2Co_7-type (hereinafter 2:7R), hexagonal Ce_2Ni_7-type (2:7H), hexagonal Pr_5Co_{19}-type (5:19H), and rhombohedral Ce_5Co_{19}-type (5:19R) phases were identified from the XRD patterns. A rhombohedral La_5MgNi_{24}-type phase (1:4R) composed of 4:1 stacking of the AB_5 and A_2B_4 units has been newly found in this work. $CaCu_5$-type phase (AB_5 phase) and C15b-$AuBe_5$-type phase (AB_2 phase) were also observed to exist. Fig. 1 shows projections onto (1, −2, 0) plane of these seven phases.

Phase abundance for the rare earth–Mg–Ni-based alloys was drastically changed with partial substitution of Ni with Mn and Al. Fig. 2 shows phase abundance of the $La_{0.8}Mg_{0.2}Ni_{3.4-x}Co_{0.3}(MnAl)_x$ alloys determined by Rietveld analysis. For the alloy without Mn and Al ($x = 0$), mass fractions of the 2:7H, 5:19R, 5:19H, and AB_5 phases were 65.5, 22.3, 7.9, and 4.3%, respectively. By partial substitution of Ni with Mn and Al, mass fraction of the 2:7H phase decreased, and those of the 5:19R and 5:19H phases increased. In the alloy with $x = 0.15$, the ratio of the 5:19H phase was more than 70%. In the alloy with $x = 0.2$ the 1:4R phase became dominant instead of the 5:19H phase. In the further substitution to $x > 0.2$ mass fraction of the

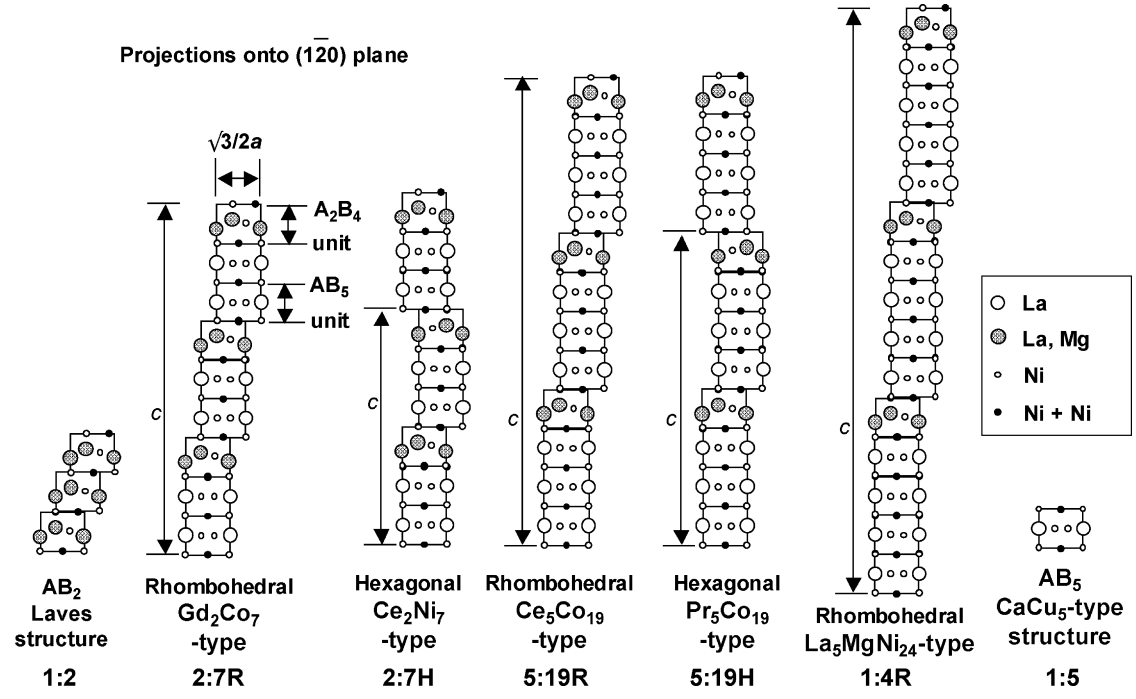

Fig. 1. Projections onto (1 $\bar{2}$ 0) plane of crystal structures observed in $La_{0.8}Mg_{0.2}Ni_{3.4-x}Co_{0.3}(MnAl)_x$ ($0 \le x \le 0.4$) alloys.

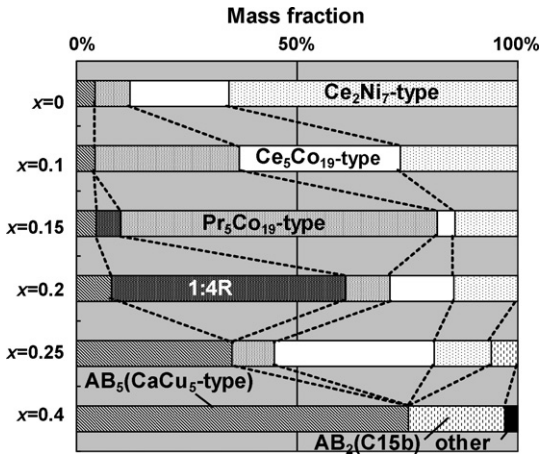

Fig. 2. Phase abundance of $La_{0.8}Mg_{0.2}Ni_{3.4-x}Co_{0.3}(MnAl)_x$ ($0 \le x \le 0.4$) alloys obtained by Rietveld refinement.

stacking-structured phases was decreased and those of the AB_5 and AB_2 phases was increased. The alloy with $x = 0.4$ contained no stacking-structured phases.

Fig. 3 shows results of Rietveld refinements for the alloy with $x = 0.2$. Fig. 4 shows crystal structure of the 1:4R phase drawn with VICS-II developed by Momma and Izumi. In the 5:19H and 1:4R phases, Mg occupies preferentially La sites in the A_2B_4 units (4f2 sites in the 5:19H phase and 6c3 sites in the 1:4R phase), and Al occupies preferentially Ni sites between the A_2B_4 and AB_5 units (12k1 sites in the 5:19H phase and 18h1 sites in the 1:4R phase) or those between the AB_5 units (12k1 sites in the 5:19H phase and 18h2 sites in the 1:4R phase). Stabilization of the 5:19H and 1:4R phases at the narrow composition range would be ascribed to the preferential occupation of Mg and Al in the particular sites.

Fig. 5 shows *P–C–T* (pressure–composition isotherm) curves of the $La_{0.8}Mg_{0.2}Ni_{3.4-x}Co_{0.3}(MnAl)_x$ alloys at 80 °C. Hydrogen storage capacity of the alloy with $x = 0.4$ was about H/M = 0.8, which was comparable to the conventional AB_5-type alloys [14]. With decreasing Mn and Al content, hydrogen storage capacity increased. The alloy with $x = 0.1$ showed capacity

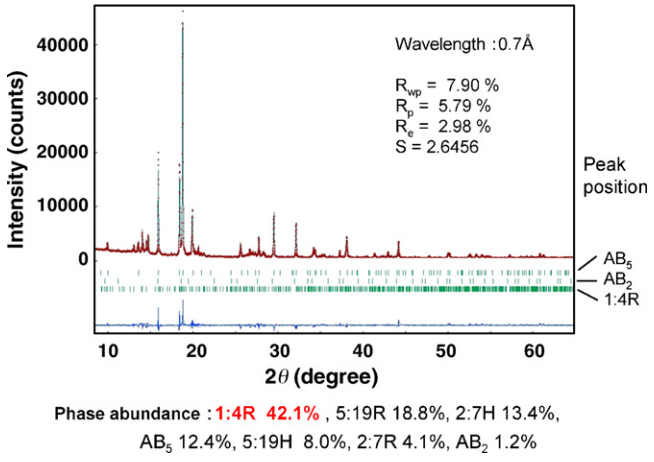

Fig. 3. Rietveld refinement pattern with synchrotron XRD pattern for $La_{0.8}Mg_{0.2}Ni_{3.2}Co_{0.3}(MnAl)_{0.2}$ alloy.

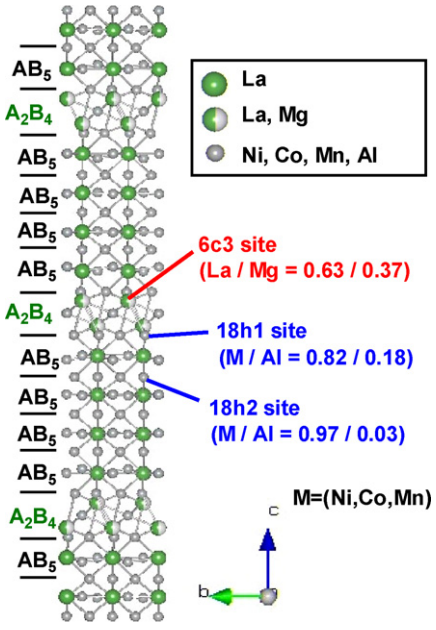

Fig. 4. Crystal structure of 1:4R (La_5MgNi_{24}-type) phase drawn with VICS-II.

of about H/M = 1.0, which was 1.2 times as high as the conventional AB_5-type alloys. Decreasing content of Mn and Al caused a decrease in lattice volume of the alloy phases, and then an increase in plateau pressure, because atomic radius of Mn and Al was larger than that of Ni. The alloy with $x = 0.2$ showed the most suitable hydrogen storage properties with high capacity and moderate plateau pressure.

The XRD pattern of the $La_{0.8}Mg_{0.2}Ni_{3.2}Co_{0.3}(MnAl)_{0.2}$ alloy after hydrogen absorption showed peak shift to lower angle without any peak separation, suggesting that each phase absorbed hydrogen with keeping their crystal structure. Table 1 shows increase in lattice parameters and lattice volume of the alloy phases during hydrogen absorption. Lattice expansion in the *a*-axis direction was 6.0–6.1% for all the phases. Lattice expansion in the *c*-axis direction was 4.2, 6.8, and 7.7% for the AB_5, 5:19R, and 2:7H phases, respectively: increased with decreasing number of the AB_5 unit in stacking structure. Average volume expansion of the alloy was estimated to be 19.7% on the basis of volume expansion ratio, mass fraction, and density of each phase. This value is much higher than that of the practi-

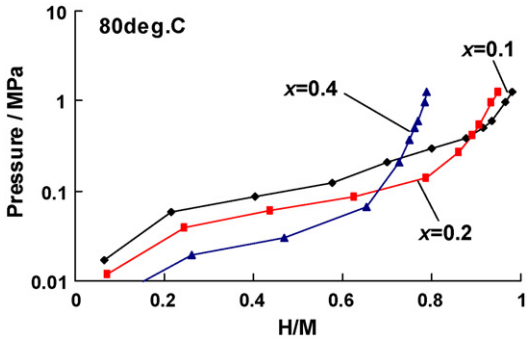

Fig. 5. PCT curves of $La_{0.8}Mg_{0.2}Ni_{3.4-x}Co_{0.3}(MnAl)_x$ ($x = 0.1$, 0.2, and 0.4) alloys at 80 °C.

Table 1
Lattice parameters before and after hydriding of AB_5, 1:4R, 5:19R, and 2:7H phases of $La_{0.8}Mg_{0.2}Ni_{3.2}Co_{0.3}(MnAl)_{0.2}$ alloy

Alloy phase	Before hydriding			After hydriding			Increase		
	a (Å)	c (Å)	V (Å^3)	a (Å)	c (Å)	V (Å^3)	Δa (%)	Δc (%)	ΔV (%)
AB_5	5.0553(4)	4.0230(3)	89.03	5.3583(5)	4.1924(4)	104.2	6.0	4.2	17.0
1:4R	5.0577(2)	60.679(1)	1344.2	5.3676(3)	64.495(3)	1609.2	6.1	6.3	19.7
5:19R	5.0588(4)	48.647(3)	1078.1	5.3663(7)	51.963(6)	1295.9	6.1	6.8	20.2
2:7H	5.0640(4)	24.426(2)	542.5	5.3719(6)	26.303(3)	657.3	6.1	7.7	21.1

cal $MmNi_5$-based alloy (11.7%) [14], but is lower than that of $LaNi_5$ alloy (24.0%) [15].

Fig. 6 shows relationship between discharge capacity and cycle number of the electrodes using the $La_{0.8}Mg_{0.2}Ni_{3.4-x}Co_{0.3}(MnAl)_x$ alloys. The alloy with $x = 0.4$ showed relatively low discharge capacity of about 300 mAh/g and poor cycle life. With decreasing content of Mn and Al to $x = 0.2$, discharge capacity increased to about 350 mAh/g, and cycle life was also improved. Further decrease in content of Mn and Al caused the decrease in initial discharge capacity and capacity retention during cycles. The alloy with $x = 0.2$ showed the most suitable electrode properties in terms of capacity and durability. The alloy with $x = 0.4$ consisting of only the AB_5 and AB_2 phases, showed lower maximum capacity and faster capacity fading than the alloys consisting of mainly the stacking-structured phases. The AB_5 phase has relatively low capacity, while the AB_2 phase has relatively large volume expansion during hydrogen absorption and shows rapid cycle degradation. In the stacking structures of the AB_5 and A_2B_4 units, it is assumed that volume expansion of the A_2B_4 unit in the a-axis direction is reduced compared to that of the AB_2 phase, and that hydrogen storage capacity is larger than the total capacity of the AB_5 and AB_2 phases, because large amount of hydrogen is absorbed not only inside the A_2B_4 units but also between the AB_5 and A_2B_4 units.

Effect of partial substitution of La with the other rare earths on crystal structure and electrode properties was investigated. Fig. 7 shows phase abundance of the $La_{0.6}RE'_{0.2}Mg_{0.2}Ni_{3.25}Co_{0.3}(MnAl)_{0.2}$ (RE′: La, Pr, and Y) alloys. Their phase structures were dependent on the substituting elements. The 1:4R phase was dominant for the non-substituted alloy, while the 5:19H and 2:7H phases became dominant for the Pr- and Y-substituted alloys, respectively. Mass fraction of the AB_5 phase in the Pr- and Y-substituted alloys was smaller than that in the non-substituted alloy. The SEM-EPMA analysis also indicates that the Pr- and Y-substituted alloys contain less amount of segregated Mg than the non-substituted alloy. Table 2 shows maximum discharge capacity and capacity retention after 50 cycles of the electrodes for the non-substituted, Pr- and Y-substituted alloys. These alloys showed similar maximum discharge capacity, but the capacity retention was improved significantly by the Pr-substitution. This effect could be ascribed to the suppression of corrosion due to the Mg segregated in the alloy.

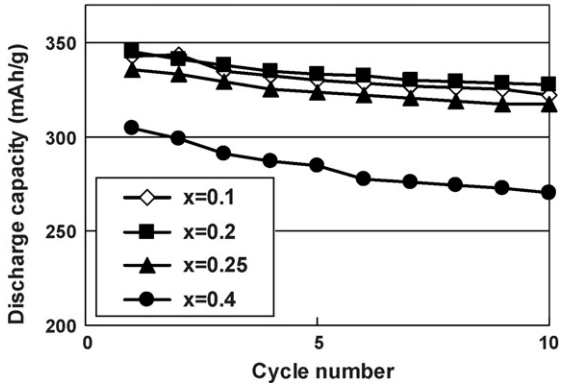

Fig. 6. Relationship between discharge capacity and cycle number of $La_{0.8}Mg_{0.2}Ni_{3.4-x-y}Co_{0.3}Mn_xAl_y$ alloy electrodes.

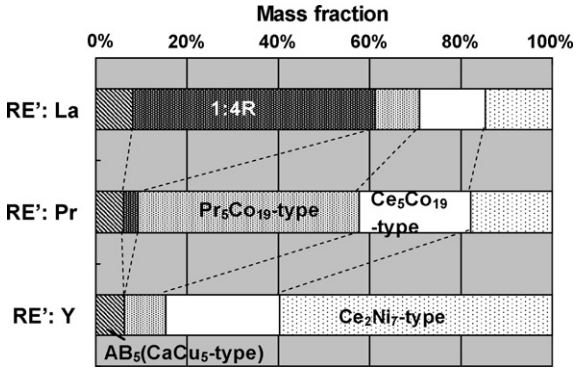

Fig. 7. Phase abundance of $La_{0.6}RE_{0.2}Mg_{0.2}$ $Ni_{3.2}Co_{0.3}(MnAl)_{0.2}$ (RE = La, Pr, and Y) alloys obtained by Rietveld refinement.

4. Conclusion

By means of synchrotron X-ray diffraction measurements and Rietveld analysis, detailed crystal structure of the rare earth–Mg–Ni-based alloys was studied. Phase structures of the $La_{0.6}RE'_{0.2}Mg_{0.2}Ni_{3.4-x}Co_{0.3}(MnAl)_x$ alloys were drastically changed by partial substitution of La with the other rare earth

Table 2
Electrochemical properties of the $La_{0.6}RE_{0.2}Mg_{0.2}Ni_{3.2}Co_{0.3}(MnAl)_{0.2}$ alloy electrodes, where C_{10} and C_{50} are discharge capacity of 10th and 50th cycle, respectively

RE	Maximum discharge capacity, C_{max} (mAh/g)	Cycle number needed for activation	Capacity retention, C_{50}/C_{10} (%)
La	345.3	1	96.0
Pr	347.9	1	98.4
Y	348.7	1	96.9

elements and of Ni with Mn and Al. Result of the Rietveld refinement suggests that the 5:19H and 1:4R stacking-structured phases are stabilized by preferential occupation of Mg and Al in the particular sites. Electrode properties such as discharge capacity and cycle life were also changed according to the change in the phase structure. The alloys consisting of mainly the stacking-structured phases showed higher maximum capacity and slower capacity fading than the alloy consisting of only the AB_5 and AB_2 phases. The $La_{0.6}Pr_{0.2}Mg_{0.2}Ni_{3.2}Co_{0.3}(MnAl)_{0.2}$ alloy showed high capacity of about 350 mAh/g and good capacity retention of more than 98% after 50 cycles. These results suggest the high possibility to develop new alloys with superior discharge capacity and cycle life by designing alloy composition and phase structures.

Acknowledgement

The authors are sincerely grateful to Ms. A. Kitano (Japan Synchrotron Radiation Research Institute) for synchrotron X-ray diffraction measurements.

References

[1] K. Kadir, T. Sakai, I. Uehara, J. Alloys Compd. 257 (1997) 115.
[2] K. Kadir, T. Sakai, I. Uehara, J. Alloys Compd. 287 (1999) 264.
[3] K. Kadir, T. Sakai, I. Uehara, J. Alloys Compd. 302 (2000) 112.
[4] T. Sakai, K. Kadir, M. Nagatani, H. Takeshita, H. Tanaka, N. Kuriyama, I. Uehara, Abstract of the 40th Battery Symposium, Kyoto, Japan, 1999, p. 133, abstract no. 1B26.
[5] J. Chen, H.T. Takeshita, H. Tanaka, N. Kuriyama, T. Sakai, I. Uehara, M. Haruta, J. Alloys Compd. 302 (2000) 304.
[6] J. Chen, N. Kuriyama, H.T. Takeshita, H. Tanaka, T. Sakai, M. Haruta, Electrochem. Solid State Lett. 3 (6) (2000) 249.
[7] H.G. Pan, Y.F. Liu, M.X. Gao, Y.Q. Lei, Q.D. Wang, J. Electrochem. Soc. 150 (5) (2003) A565–A570.
[8] T. Kohno, H. Yoshida, F. Kawashima, T. Inaba, I. Sakai, M. Yamamoto, M. Kanda, J. Alloys Compd. 311 (2000) L5.
[9] S. Yasuoka, Y. Magari, T. Murata, T. Tanaka, J. Ishida, H. Nakamura, T. Nohma, M. Kihara, Y. Baba, H. Teraoka, J. Power Sources 156 (2006) 662.
[10] H. Hayakawa, E. Akiba, M. Gotoh, T. Kohno, Mater. Trans. 46 (2005) 1393.
[11] T. Ozaki, Y. Kitano, S. Tanase, T. Sakai, M. Kanemoto, T. Kakeya, M. Kuzuhara, M. Watada, ECS 208th Meeting, Los Angeles, 2005, abstract number 861.
[12] M. Kanemoto, T. Kakeya, M. Kuzuhara, M. Watada, T. Ozaki, T. Sakai, ECS 208th Meeting, Los Angeles, 2005, abstract number 852.
[13] F. Izumi, T. Ikeda, Mater. Sci. Forum 321–324 (2000) 198.
[14] H.B. Yang, T. Sakai, T. Iwaki, S. Tanase, H. Fukunaga, J. Electrochem. Soc. 150 (12) (2003) A1684–A1688.
[15] T. Sakai, K. Oguro, H. Miyamura, N. Kuriyama, A. Kato, H. Ishikawa, J. Less-Common Met. 161 (1990) 193–202.